Journal of Nuclear Materials 574 (2023) 154185

Contents lists available at ScienceDirect

Journal of Nuclear Materials

journal homepage: www.elsevier.com/locate/jnucmat

Grain growth kinetics of the gamma phase metallic uranium

Dong Zhao[a], Michael T. Benson[b], Kun Yang[a], Yonglin Huang[a], Fidelma G. Di Lemma[b], Bowen Gong[a], Fudong Han[a], Jie Lian[a,*]

[a] Department of Mechanical, Aerospace, and Nuclear Engineering, Rensselaer Polytechnic Institute, Troy, NY, USA, 12180
[b] Idaho National Laboratory, P.O. Box 1625, MS 6188, Idaho Falls, ID 83415

ARTICLE INFO

Article history:
Received 8 June 2022
Revised 29 November 2022
Accepted 30 November 2022
Available online 2 December 2022

Key words:
Gamma phase uranium
Grain growth kinetics
Triple-junction migration

ABSTRACT

Metallic uranium is a leading fuel form for sodium cooled fast reactors as an enabling technology of future nuclear energy systems. Mechanistic understanding of fuel behaviors and kinetics under thermodynamic equilibrium and highly non-equilibrium conditions are essential for evaluating fuel performance. It is important to understand and predict the grain and pore evolutions of metallic fuels under thermal and irradiation conditions. However, very limited data are available on the grain growth kinetics and mechanisms of pure gamma phase uranium. In this paper, the pure gamma uranium pellets with different grain structures were fabricated by combining high-energy ball milling and spark plasma sintering. Isothermal annealing tests were performed to investigate the grain growth behavior of the pure gamma phase uranium with different initial grain sizes. A parabolic relationship in grain growth with time was identified for the submicron-sized (374 nm) sample. In contrast, for the nano-sized (137 nm) sample, the grain growth shows a linear relationship with time. The activation energies of grain growth were determined as 199.5 KJ/mol and 80.6 KJ/mol for nano-sized and submicron-sized grain structures, respectively. For the nano-sized sample, the rate-control step of grain growth is dominated by the triple-junction migration, in which the grain boundary triple junction drags the grain growth, leading to a higher activation energy than the bulk diffusion. The dominating mechanism for the submicron-sized sample is grain boundary diffusion. The mechanistic understanding and critical data obtained on the kinetics of pure uranium phases will be useful to evaluate fuel behavior under thermodynamic equilibrium conditions and develop a high fidelity model to predict fuel performance.

1. Introduction

The metallic nuclear fuel (e.g., U-Pu-Zr and U-Zr) is the leading fuel form for sodium-cooled faster reactors because of multiple advantages, such as its high thermal conductivity, high fissile element densities and low fabrication cost [1]. However, two issues encountered for metallic fuels limit their burnup potential, including fuel-cladding chemical interaction (FCCI) and fuel-cladding mechanical interaction (FCMI). FCCI can be mitigated by adding Zr to the fuel slug, slowing down the inter-diffusion between the fuel and cladding constituents [2]. The FCMI can be mitigated by a low smear density fuel slug design, in which the diameter of the fuel slug is smaller than that of the cladding tube and the gap between them is filled by high thermally-conductive materials such as sodium. With a low smear density, FCMI can be mitigated to increase fuel burnup up to 15–19 at.% without cladding breach [3,4]. Nevertheless, the sodium bonded spent fuels are hazardous and require a costly process to remove the sodium before disposal. To eliminate sodium bonding, an alternative annular fuel design has been reported by Idaho National Laboratory (INL) [5], in which the small gap between fuel and cladding can be bonded by helium instead of sodium. Numerous steady-state irradiation experiments and post-irradiation examinations have been performed to investigate the irradiation behavior of metallic fuels with different designs. For both annular U-Zr [6] and sodium bonding U-Pu-Zr [7] fuels, constituent redistribution has been observed, induced by the temperature gradient inside the fuel. The center-line temperature of metallic fuels is higher than 933 K and gamma phase uranium is one of the major phases of metallic fuels during reactor operation [7]. As a result, metallic fuels are utilized in complex environments of intensive radiation and temperature gradient coupled with complexities of elemental redistribution, phase and microstructure evolution.

Fundamental thermodynamic behaviors of different phases of metallic fuels will be essential to understanding the phase behavior and fuel properties under highly non-equilibrium conditions experienced during reactor operation. Of particular importance,

* Corresponding author.
E-mail address: lianj@rpi.edu (J. Lian).

https://doi.org/10.1016/j.jnucmat.2022.154185
0022-3115/

the thermodynamic behavior of gamma phase uranium, especially grain growth under isothermal annealing, is necessary for understanding and predicting the grain structure evolution (grain size, pore etc.) and subsequent swelling of metallic fuels induced by thermal and radiation processes inside the reactor. However, only limited data on thermodynamic behavior and properties of gamma phase pure uranium are available. For example, gamma phase uranium is a high-temperature phase (from 1042 K to 1403 K) with a body-centered cubic structure [8,9]. Adda et al. measured diffusion coefficient ($D_0 = 1.8 \times 10^{-3}$ cm^2/sec) and an activation energy ($Q = 27.5$ kCal/mol) of pure gamma phase uranium by using diffusion couples made of natural uranium and uranium enriched with U^{234} [10]. In addition, limited mechanical properties such as Young's modulus and high temperature creep behaviors were previously reported [11,12]. Currently, the research related to the gamma phase uranium is usually performed within the context of uranium alloys, such as U-Zr, U-Mo, and U-Nb, etc. [13]. Thus, there is no experimental data available on the grain growth behavior of the pure uranium gamma phase under isothermal annealing.

In this study, dense pure gamma phase uranium pellets were prepared by spark plasma sintering (SPS) and the microstructure was controlled by different SPS sintering and thermal treatment conditions with the grain structures varying from nano-scale to sub-micron scale, serving as the model systems to investigate the grain growth kinetics of the gamma phase by isothermal treatment. With the synchronous current field and pressure assistance, the SPS is an effective powder sintering method with a high heating rate and controllable cooling [14,15]. Unlike traditional sintering methods, i.e., powder sintering or hot pressuring, the high pulsed DC passes through the graphite die and metallic powders, and the induced Joule heating and plasma accelerate the necking formation, densifying the sample in a short time under relatively low temperatures. Thus, SPS is an ideal method for sintering highly densified samples with controlled microstructure (e.g., from nano-sized to micro-metered scales) or metastable phases etc. [16]. The high energy ball milling (HEBM) and SPS have been used to fabricate nano-sized and submicron-sized polycrystalline pure uranium. Isothermal annealing with different temperatures has been performed to investigate the grain growth mechanisms and kinetics of the gamma phase pure uranium with different starting grain structures. For the submicron-sized gamma phase uranium, grain boundary diffusion dominates the grain growth rate, and the grain growth exponent equals to 2. However, for the nano-sized gamma pure uranium, the grain growth exponent is 1, dominated by the movement of the triple junctions. The activation energy of triple junction movement is determined to be greater than that of grain boundary diffusion. These basic thermodynamic properties and kinetics of the gamma phase uranium are useful for the evaluation of the fuel behavior under relevant thermal environment of reactor operation and the simulation and prediction of metallic fuel performance.

2. Experimental

In this work, pure uranium powders were prepared by INL using a hydride-dehydride process on bulk metallic uranium. The as-received powders were processed by HEBM equipment (Pulverisette 7, Idar-Oberstein, Germany) to obtain highly plastic deformed powder agglomerates consisting of smaller particles with different particle sizes of nano- and micro-sized crystals for thermal treatment by controlling ball milling times of 10 hrs and 20 hrs. Specifically, for the nano-sized uranium precursor powders, 20 hrs of ball milling was used with the 1.8 mm WC milling balls, and the ball milling speed was kept as 250 rpm. For the submicron-sized uranium precursor powders, 10 hrs of ball milling was used with 8 mm WC milling balls, and the ball milling speed was 500 rpm. To prevent overheating of powders during the ball milling process, milling was paused for 10 min for each 15 min milling cycle. After HEBM and particle size refinement, the powders were loaded into a WC ball milling jar inside a glovebox with an oxygen level lower than 10 ppm. A SPS apparatus (Fuji, Dr. Sinter SPS 211-LX, Saitama, Japan) was used to sinter the loosely-packed powders into a compacted geometry suitable for post thermal treatment and isothermal annealing. All samples were sintered in 8 mm graphite dies, and hydrostatic pressure of 40 MPa was applied during the SPS consolidation. The heating rate was 150 K/min, and the sintering temperatures were 873 K for 10 h-ball milling powders and 973 K for 20 h-ball milling powders, respectively, with a thermal holding time of 3 min.

The isothermal annealing of pure U samples for investigating grain growth kinetics was conducted in a muffle furnace with different temperatures (1073, 1173, and 1273 K) and different durations (5 to 25 hrs), and the heating rate to the target temperature was 10 K/min. The choose of annealing temperatures is based on the phase diagram of pure uranium, in which gamma phase uranium exists between 1049 K to 1408 K [17]. Isothermal annealing at different durations and temperatures have been conducted to elucidate the grain growth mechanisms and activation energies. Samples were cooled in the furnace to room temperature after thermal annealing. To avoid exposure to air and prevent oxidation during isothermal annealing, the U samples were covered with a Ta foil and loaded into quartz tubes inside the glovebox. Then the quartz tubes containing samples were connected with a valve on the open end with a high vacuum Swagelok union. The quartz tube loaded with uranium pellets was then taken out from the glovebox and purged three times with ultra-high purity Argon by a purging system and then the quartz tube was pumped to 50 milli-torrs and sealed by oxyhydrogen flame. Before the annealing test, a piece of Ta foil loaded inside the quartz tube was heated to around 1273 K by the torch to absorb the residual oxygen inside the tube. Thus, the samples have not been exposed to air for the whole process. After isothermal annealing, the microstructure of samples was characterized by a scanning electron microscope (SEM, Carl Zeiss Supra 55, Germany), and the grain structure was analyzed by ImageJ. The grain structure evolution of pure uranium pellets upon isothermal annealing was characterized, and the average pore and grain sizes were determined. For each sample, at least 150 grains were measured to obtain average grain size and statistical grain size distribution.

3. Results

3.1. SPS consolidation and microstructure of submicron (374 nm) and nano-sized (137 nm) pure uranium pellets

Compacted pure uranium pellets were produced by SPS from the submicron-sized and nano-sized uranium powders subjected to 10 hrs or 20 hrs ball milled powders, and the ball milling time was the critical parameter to control the starting grain size of the pellets for isothermally-induced grain coarsening behavior. Particularly, highly plastically deformed powders were produced by 10 hr-ball milling, resulting in a submicron-sized grain structure for the pellet consolidated by SPS under 873 K and 40 MPa (Fig. 1A). The fracture surface of the as-sintered pellet and the close-up view (inset in Fig. 1A) show plastic deformation of the fracture surface, and no grain or grain boundary are observed. Fig. 1D shows highly plastically deformed uranium powders after 20 hrs-ball milling. After SPS sintering under 973 K and 40 MPa, the sintered pellets show compaction of the large-sized and highly plastically deformed agglomerates without minimized neck formation and significant densification during the SPS sintering with the assistance of current flow and high pressure. With the SPS short sinter-

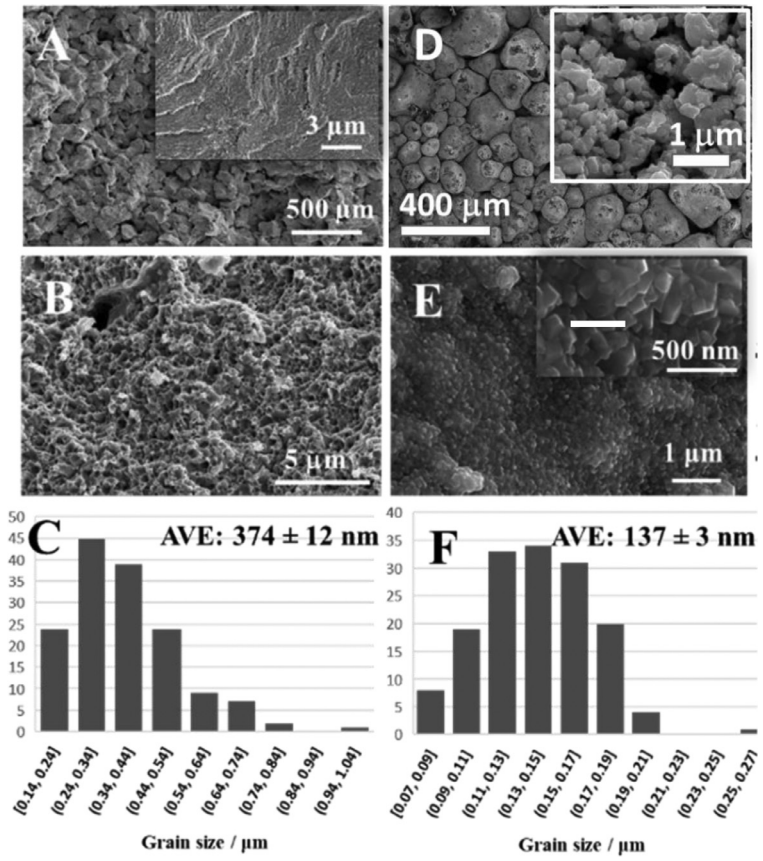

Fig. 1. Surface morphology and microstructure of the SPS consolidated pellets from pure uranium powders ball milled with different durations (A (as-sintered) and B (annealed) for the 10 h ball milling sample, and D (as-sintered) and E (annealed) the 20 h ball milling sample). SPS sintering was conducted at 973 K, 40 MPa and 10 min, and the post SPS thermal annealing was performed at 1073 K for 5 h. Grain size distributions for 10 h and 20 h ball milling samples are shown in C and F, respectively.

ing, the highly plastically deformed particles maintain a stable internal structure and well-maintained structural integrity, allowing isothermal annealing and microstructure characterization for grain coarsening investigation.

In order to study the grain coarsening kinetics, the highly plastically deformed samples were first annealed at 1073 K for 5 hrs to obtain the micron- and nano-sized microstructure through the recrystallization. The plastic damage and defects can be recovered and new grains form upon isothermal thermal annealing, leading to well crystallized microstructures, significantly improved crystallinity and densification. For 10 hrs ball milling samples, the intergranular fracture surface showed equiaxed grains at the submicron-sized regime. For 20 hrs ball milling samples (as shown in Fig. 1E), nano-sized faceted grains (137 nm) formed. Here, the nano-sized structure refers to the sample sintered from the powders ball milled for 20 hrs and submicron-sized structure refers to the sample sintered from powders ball milled for 10 hrs. Figs. 1C and F show the grain size statistic distribution for 10 hrs and 20 hrs ball milling sample respectively, and both show a lognormal distribution. Fig. 2 shows the XRD results of the annealed samples at 1073 K for 5 hrs synthesized with different ball milling durations. Both samples showed relatively low X-Ray intensity because of the small grain size and low penetration depth of X-Ray in uranium [18]. The dominant alpha uranium phase is observed, which is the stable phase of pure uranium at room temperature. Minimized oxide impurity phases (e.g., from UO_2 and UO) are also observed, and the UO_2 phase can be attributed to the surface oxidation resulting from air exposure of the samples removed from quartz tubes for XRD tests. UO phase may be induced by the surface oxidation of the pure metallic phase during

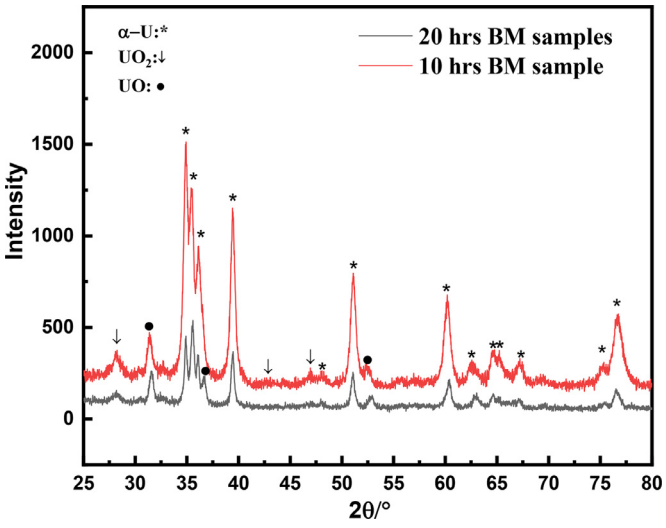

Fig. 2. X-ray diffraction patterns of the pure metallic uranium after isothermal annealing at 1073 K for 10 hrs showing dominant alpha uranium with minimal oxide impurity phases post isothermal annealing.

isothermal thermal annealing at high temperature. However, the UO phase only formed under trace concentration of O_2 [19,20]; thus, the formation of UO phase can also demonstrate the low concentration of oxygen inside the quartz tube during the annealing. These results clearly imply that high purity of the environment inside the quartz tube during the isothermal annealing testing, and

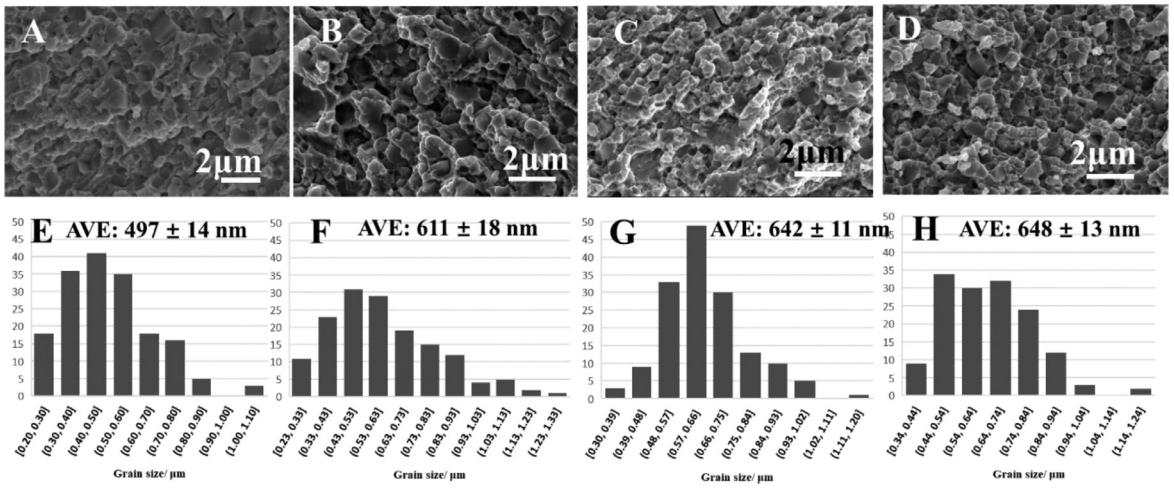

Fig. 3. Fracture morphology and grain size distribution for 10 hrs BM sample with different annealing durations under 1073 K (A, E: 5 hr; B, F: 10 hrs, C, G: 15 hrs; D, H: 20 hrs).

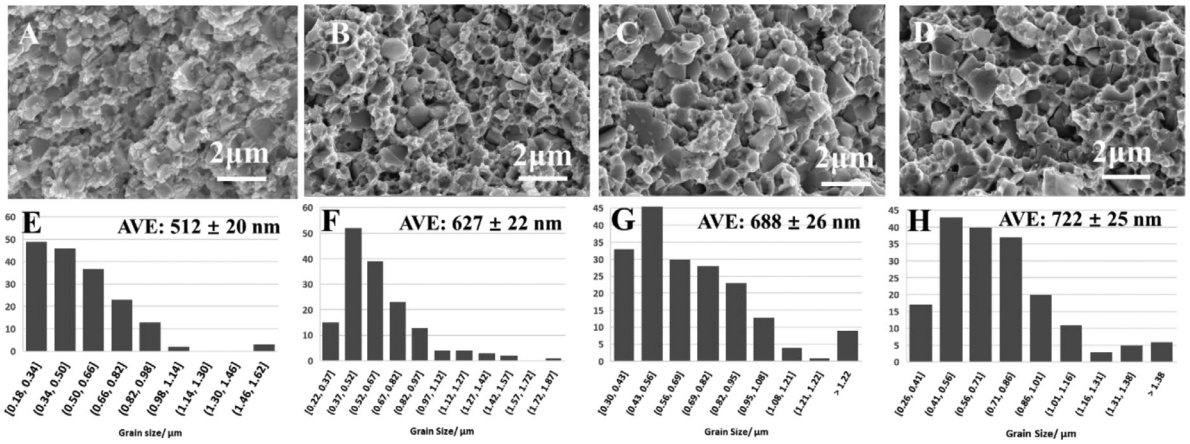

Fig. 4. Fracture morphology and grain size distribution for 10 hrs BM sample with different annealing durations under 1173 K (A, E: 5 hr; B, F: 10 hrs, C, G: 15 hrs; D, H: 20 hrs).

the gamma phase is the dominant phase when annealed at high temperatures of 1073 ~ 1273 K.

3.2. isothermal annealing of sub-micro and nanocrystal pure uranium samples

The well-crystallized grain structures of the pure uranium pellets post SPS sintering and thermal treatment served as the model system for systematic investigation of the thermally-induced grain coarsening kinetics. Figs. 3–5 show the surface morphologies and microstructure of 10 hrs BM samples with different isothermal annealing temperatures (1073 ~1273 K) and durations (5, 10, 15 and 20 hrs). Fig. 4 shows the sample post 1073 K isothermal annealing with different durations. As shown in SEM results, the grain boundary can be clearly observed through the fractured surface. Over 150 grains are measured in order to accurately measure the average grain size. Statistical analysis of the grain size distributions of samples with different durations show a lognormal distribution of grain structure evolution upon isothermal annealing. The grains grew quickly at the initial annealing stage and then slowed down due to the loss of driving force. A similar phenomenon has been observed with higher isothermal annealing temperatures. The SEM and grain size statistic results for 1173 and 1273 K isothermal annealing are shown in Figs. 4 and 5 respectively. Under the same annealing duration, the grains grow into larger size for the samples isothermally annealed at higher temperature due to the higher grain boundary mobility.

The SEM images (Figs. 6–8) show the grain coarsening and grain size distribution of the 20 hrs BM samples upon isothermal annealing at different temperatures and durations. As shown in Fig. 6, the sample annealed under 1073 K displays nano-sized facetted grains in a cubic shape on the surface, and the growth of the nano-sized grains is much slower than micro-sized grain. The grain growth rates for the initial submicron grain-sized and nano-sized grained structures are determined as functions of isothermal annealing duration at different temperatures as shown in Fig. 9A and 9C. A parabolic growth behavior can be observed for the initial submicron sized grain structure with a rapid growth rate followed by gradual reduction and saturation at a larger grain size. For the nano-sized grains, the grain growth rate initially showed a linear relation with time and then transited to a parabolic growth behavior as the grain size reached 400 nm for the sample post 1173 K annealing test, suggesting a transition in the grain growth kinetics and mechanisms. This is against the conventional wisdom as it is expected that the nano-sized grain structure will display a greater kinetics for grain coarsening due to the larger driving force for the curvature-driven grain growth. However, our results for the nano-sized grain structure of pure gamma uranium phase suggest a critical size below which the growth kinetics is reduced. The linear grain growth kinetics with slower growth rates was previ-

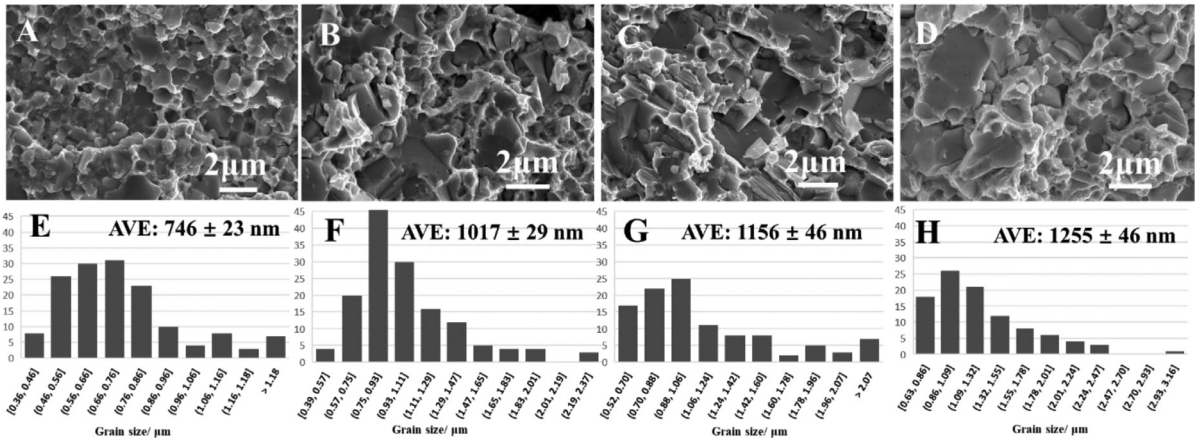

Fig. 5. Fracture morphology and grain size distribution for 10 hrs BM sample with different annealing durations under 1273 K (A, E: 5 hr; B, F: 10 hrs, C, G: 15 hrs; D, H:20 hrs).

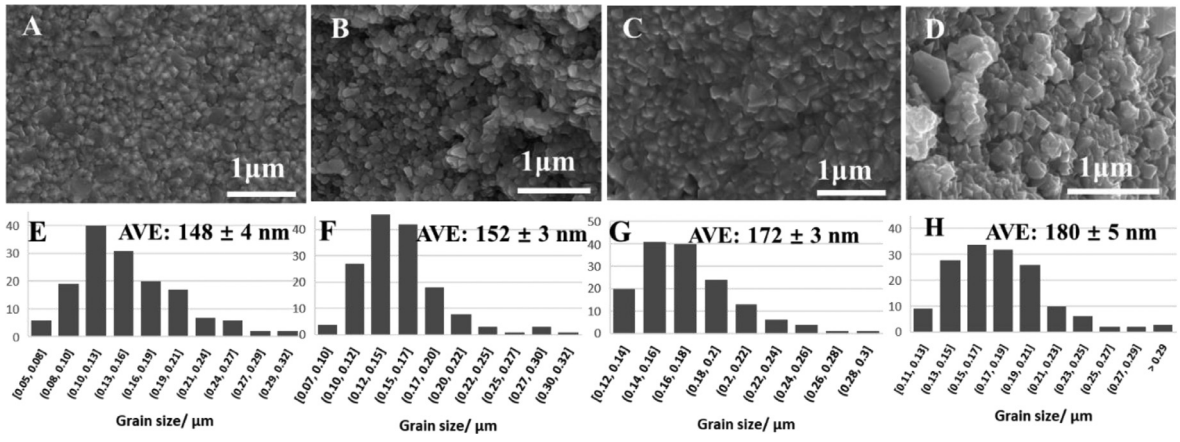

Fig. 6. Fracture morphology and grain size distribution for 20 hrs BM sample with different annealing durations under 1073 K (A, E: 5 hr; B, F: 10 hrs, C, G: 15 hrs; D, H: 20 hrs).

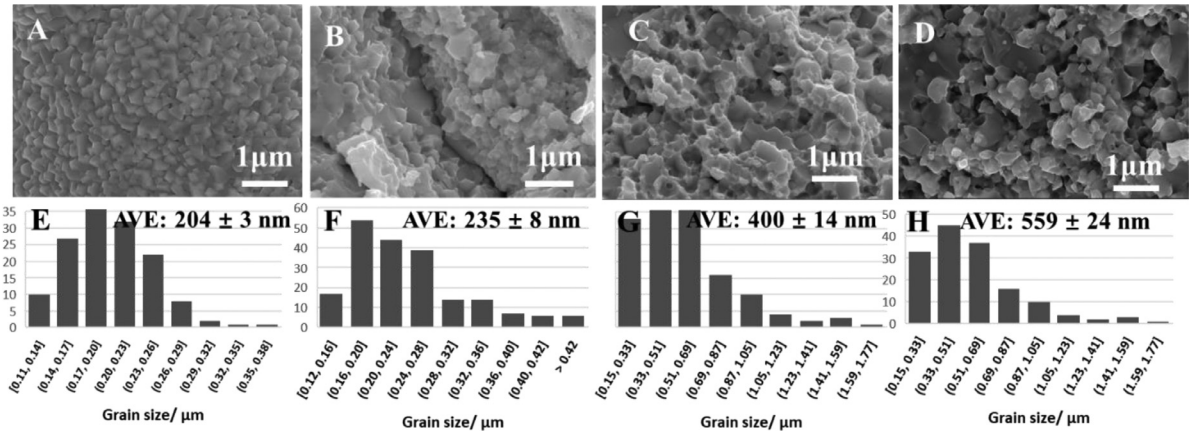

Fig. 7. Fracture morphology and grain size distribution for 20 hrs BM sample with different annealing durations under 1173 K (A, E: 5 hr; B, F: 10 hrs, C, G: 15 hrs; D, H: 20 hrs).

ously reported for nanocrystalline grains in the literature [21–23]. For the isothermal annealing test under 1273 K, the grain shape transferred from regular polygons to the irregular polygons with a rounded surface morphology, which may be induced by the higher annealing temperature. The reasons for different grain growth behavior and grain shape will be discussed in detail in the next section to analyze the grain growth kinetics and mechanisms.

3.3. Grain growth kinetics and mechanisms

The grain growth rates of the submicron-sized uranium obtained experimentally are fitted by MATLAB with 95% confidence bounds assuming a normal grain growth kinetic based on the following equation[24]:

$$D^n - D_0^n = K_0 e^{\left(\frac{-Q}{RT}\right)} t \quad (1)$$

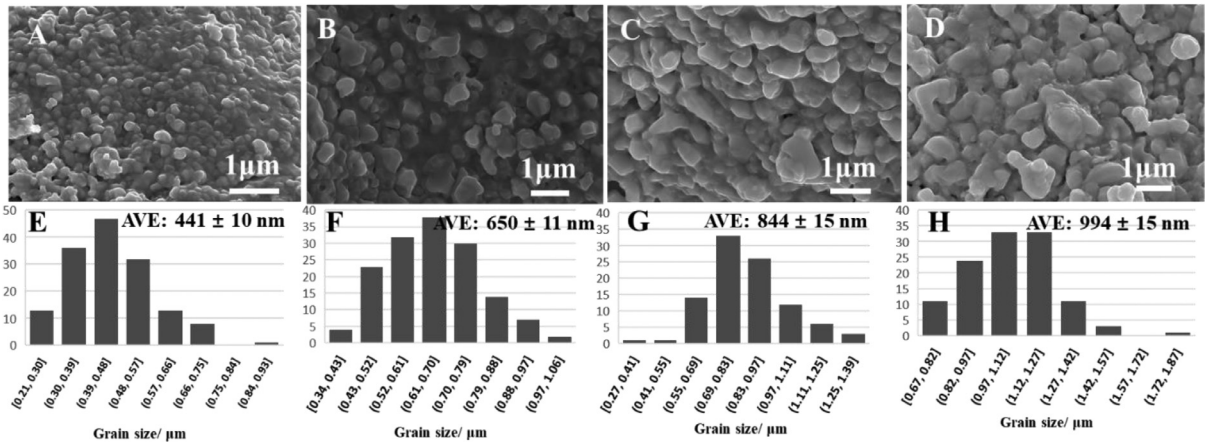

Fig. 8. Fracture morphology and grain size distribution for 20 hrs BM sample with different annealing durations under 1273 K (A, E: 5 hr; B, F: 10 hrs, C, G: 15 hrs; D, H:20 hrs).

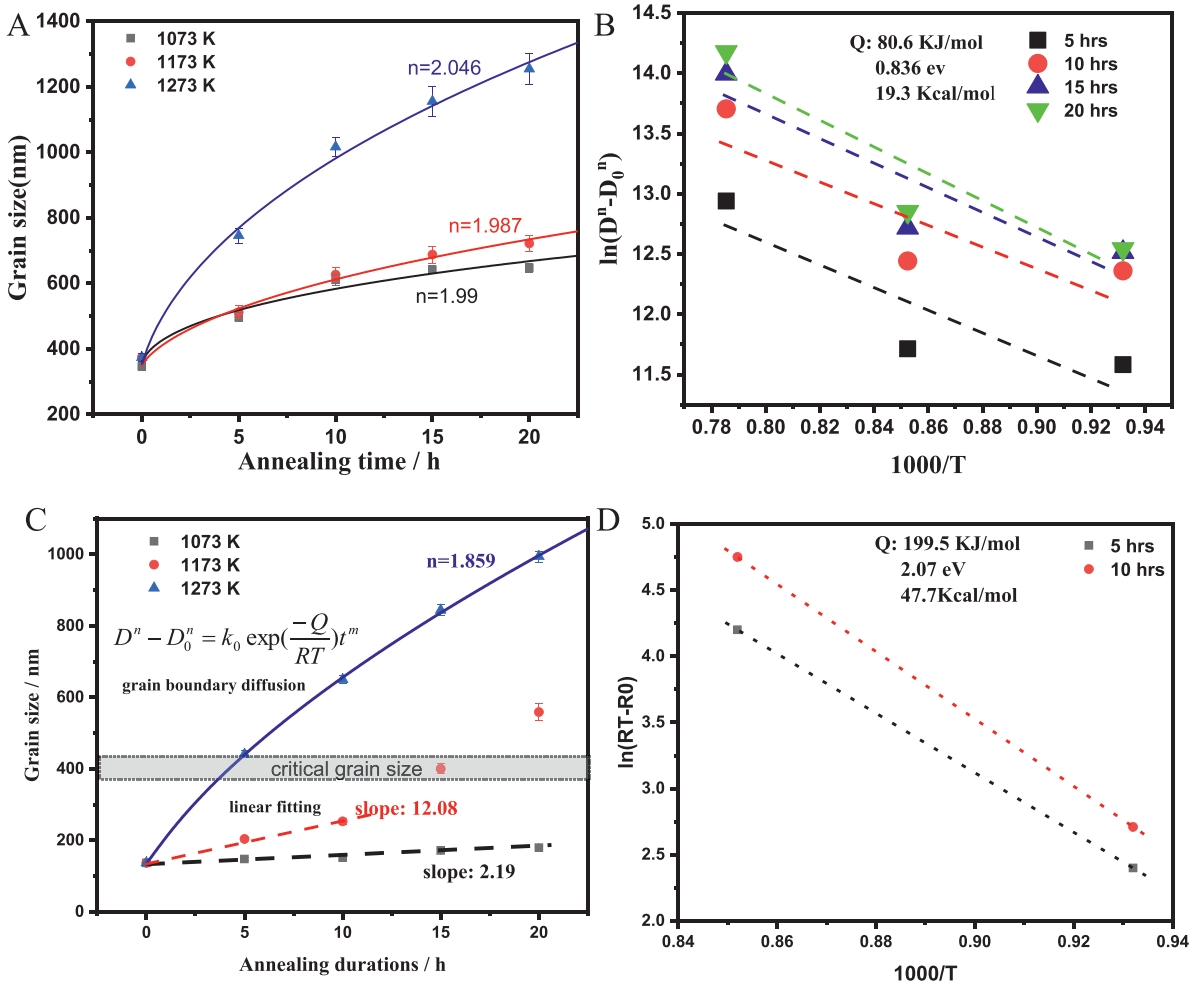

Fig. 9. A: grain growth components for submicron-sized uranium; B the activation energy of submicron-sized grain growth; C: grain growth components for nano-sized uranium; D: the activation energy of nano-sized grain growth.

in which D is the grain size of annealed uranium, D_0 is the initial grain size, n is the grain growth exponents, K_0 is a constant, Q is the activation energy, R is the gas constant, T is the absolute temperature and t is the annealing duration (hours).

The grain growth exponent of the submicron-sized uranium is determined to be 2.01 (as shown in Fig. 9A) at different annealing temperatures, which is consistent with the ideal value of the single-phase polycrystal grain growth exponent [25]. This result also demonstrates the high purity of submicron-sized uranium fabricated by HEBM and SPS. The activation energy of grain growth can be calculated through the formula (2), by linearly fitting of $ln(D^n - D_0^n)$ vs. T, as shown in Fig. 9C.

$$ln(D^n - D_0^n) = ln(K_0 t) - (Q/R)T \quad (2)$$

The activation energy of the submicron-sized grain growth is determined to be 80.6 KJ/mol (19.27 Kcal/mol), which is smaller than the activation energy of self-diffusion of gamma phase uranium measured by Y. Adda (27.5 Kcal/mol) [10], and N.L. Peterson (26.7 Kcal/mol) [26]. This result implies that the grain growth kinetics of the submicron gamma-phase uranium may be dominated by grain boundary diffusion with a substantial reduction in the activation energy as compared with self-diffusion in bulk uranium. Generally, the activation energy of diffusion on the grain boundary is usually smaller than that of bulk diffusion in the lattice [27,28].

As shown in Fig. 9C, the grain growth of nano-sized grain shows a different behavior and is sluggish in contrast to the micro-grain sized sample. The linear relationship in the grain size and annealing duration can be identified for isothermal annealing at 1073 K. Thus, a similar relationship is also observed for the sample post first 10 h of thermal annealing under 1173 K. Similar results have been observed for grain growth of nano-crystalized iron samples [20]. The linear grain growth model has been introduced in the literature [22], as shown in formula (3): [22]

$$R(t) = R_0 + \frac{yD_{SD}}{12Nk_BTZ[(\delta V)/A]^2}\mathrm{t}(\mathrm{R} < \mathrm{Rc}) \tag{3}$$

in which R(t) represents the grain size of the annealed sample; R_0 is the initial grain size; T is temperature; t is annealing duration; K_B is the Boltzmann constant; N is the number of atoms per unit volume; Z is the atomic coordination number; and δ_V is the excess volume induced by the grain boundary as compared with a single-crystalline state. D_{SD} is bulk diffusion coefficient, which can be calculated from formula (4) and D_0 is the pre-exponential factor. Formula (5) can be derived from formulas 3 and 4, from which the activation energy of bulk diffusion can be calculated. R_T represents the grain size of the sample annealed under different temperatures. [22]

$$D_{SD} = D_0 exp(-Q_{SD}/TK_B) \tag{4}$$

$$ln\left(\frac{R_{T1} - R_0}{R_{T2} - R_0}\right) = \frac{Q_{SD}}{K_B}\left(\frac{1}{T_2} - \frac{1}{T_1}\right) \tag{5}$$

Fig. 9D shows the plot for ln (R_T-R_0) with respect to 1000 times 1/T and the bulk diffusion activation energy of 199.5 KJ/mol (47.7 Kcal/mol) can be calculated from the slope, which is larger than that of self-diffusion of gamma phase uranium measured by Adda (27.5 Kcal/mol) [10], and Peterson (26.7 Kcal/mol) [26].

4. Discussion

Different grain growth mechanisms have been proposed for the linear grain growth behavior, including the bulk diffusion-controlled grain growth mechanism [29] and triple-junction migration behavior [30]. For the bulk diffusion-controlled grain growth mechanism, with the grain growth, the excess volume localized in the vanished grain boundary core regions must be accommodated elsewhere in the sample or transferred to the surface [29]. According to the previous research [25], much of the excess volume from the annihilated boundaries transfer to the vacancies near the grain boundaries. In the bulk diffusion-controlled model, the annihilation of grain boundary can be induced by the diffusion of the atoms across the grain boundary, leading to the formation of vacancies along the adjacent crystalline region of the grain boundary [25]. The high concentration of defects increases the system's Gibbs free energy, counteracting the reduction of the free energy induced by grain growth. The grain growth process can be stopped if there is a positive change of the system's free energy [29]. Thus, the rate-control step is the diffusion of vacancies to the defect sinks or the sample surface to decrease the Gibbs free energy, which is associated with the counter diffusion of uranium atoms in their sublattice to the vacant site. The activation energy in equation (4) should be the activation energy of bulk diffusion in the lattice for gamma phase uranium. Therefore, the linear growth kinetics cannot be explained by the excess volume of grain boundary model as depicted in formula (5) due to the higher activation energy than bulk diffusion.

The deviation in the activation energy from the self-diffusion and the sluggish grain growth rate could be attributed to dragging force induced by the triple junction of the grain boundary [31][30]. The dragging parameter of the triple junction can be calculated from formulas 6 and 7 for the grains with a different number of neighbors [32], in which Λ represent the dragging parameter of the triple junction to the movement of grain boundaries, and x represent the number of neighbors for polygonal grains. The $\underline{m_{tj}}$ represents the mobility of the triple junction, and the m_{gb} represents the grain boundary mobility. As shown in Fig. 10B, θ represents half of the dihedral angle in the vertex of the triple junction, σ represents the grain-boundary surface tension, and σ_b represents the grain-boundary tension of the third boundary, and d represents the grain size. The grain boundary surface tension is related to the mismatch of orientation between two grains [17] and its relative value reached a constant with a large mismatch of the angle of orientation.

$$\Lambda = \frac{m_{tj}d}{m_{gb}} = \frac{ln\ \sin\theta}{\sigma_b/\sigma\ -\ 2\cos\theta} \qquad x > 6 \tag{6}$$

$$\Lambda = \frac{m_{tj}d}{m_{gb}} = \frac{2\theta}{2cos\theta\ -\ \sigma_b/\sigma} \qquad \mathrm{x} < 6 \tag{7}$$

The dragging force parameter, Λ, can be calculated from formula 7 if the number of neighbors for polygonal grains, x, is smaller than 6. By assuming a 1:1 ratio for the surface tension between grain boundary 3 and boundary 1, Λ is decreased with decreasing the dihedral angle in the vertex of the triple junction, meaning the dragging force of the triple junction is large enough to make the grain growth rate for gamma uranium sluggish. For the grain with $x > 6$, Λ is approaching infinitesimal with the dihedral angle close to $\pi/2$ and approaching infinity when the dihedral angle equals to $\pi/3$.

As shown in Fig. 10A, the grains of the 20 hrs ball milled sample show the stacking of polygonal grains with quadrilateral and pentagonal shapes with sharp vertexes from 2D views. The intersections of quadrangles form triple junctions along the grain boundary, and the vertex of the junction is smaller than that of the junction formed by hexagonal shape grains. The triple junction motion-controlled grain growth theory predicts that the grain boundaries will become flat and grains approach a shape of equilateral polygons if the grain growth is controlled by the triple-junction [33]. Thus, the polygonal shape of nano-sized uranium shown in Fig. 10A implies additional mechanisms of the triple junction controlling grain growth for nano-sized crystalline gamma phase uranium.

$$A = m_{tj}\sigma d = A^0_{tj} exp\left(-\frac{Q_{tj}}{KT}\right) \tag{8}$$

With the limited mobility of grain boundary triple junctions, the grain growth exponent, n shown in Eq. (2), decreases to 1. Thus, the grain growth rate can be fitted by a linear model as shown in formula (8) [32], in which A represents the grain boundary velocity with triple junction, and Q_{tj} represents the activation energy of the triple junction motion, and A^0_{tj} represents the coefficient of the triple-junction grain boundary velocity. Therefore, Q_{tj} can be calculated from formula (5), which is 47.7 Kcal/mol as shown in Fig. 9D, larger than the activation energy for lattice diffusion and grain boundary diffusion for gamma phase uranium. The

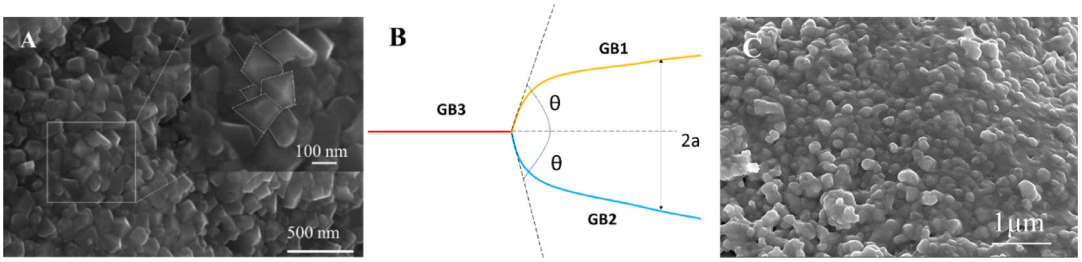

Fig. 10. (A) A SEM image and a large view (inset in the Figure 11 A) for the 20 h BM pure uranium upon isothermal annealing at 1073 K for 5 hrs showing a quadrilateral grain geometry; (B) a schematic diagram showing the triple junction; (C): a round shaped grain geometry for the 20 h BM pure uranium upon isothermal annealing at 1173 K for 5 hrs, clearly showing the transition from the originally quadrilateral grain geometry upon high isothermal annealing at higher temperatures and elongated durations.

larger activation energy for triple junction than grain boundary diffusion and bulk diffusion has also been reported by Sursaeva et al. [32]. Thus, the triple-junctions migration is the rate-controlling step for the grain growth of the nano-sized gamma phase uranium, rather than the excess volume mechanism reported by C.E. Krill et al. [22].

At longer annealing durations or higher annealing temperatures, the shape of grains evolved from a quadrangle geometry to a hexagon or more-rounded shaped polygon with a larger θ. Thus, the dragging force induced by triple junctions can be mitigated due to the change of θ under higher isothermal annealing temperatures as shown in Figs. 10A and C. The dependence of θ on temperature has been discussed and demonstrated by Czubayko et al. [34]. When the temperature nears the melting temperature, θ tends to the value of thermodynamic equilibrium and the Λ is approaching infinity [34]. Thus, for the nano crystallized sample annealed under 1000 °C, the motion of grain boundary is independent of the triple junction mobility and the grain growth exponent is close to 2, in which the growth kinetics is similar to the submicron-sized grains as described in formula (1).

While the model of limiting movement of the triple junction has been developed and demonstrated by multiple experiments and simulation results, there is no complementary mechanistic explanation [30,33–35]. The plausible explanation [31] is from the atomistic theory of grain boundary mobility [36], in which the grain boundary migration is controlled by the motion of atoms from shrinking grain boundary areas to the growing grains. In this process, the atoms are dissociated from the kink to a position on the step firstly, and then diffuse along the step until dissociated from the step to the surface of the grains. After that, the dissociated atoms can diffuse along the surface until condensed on the surface of growing grains. In conclusion, the grain boundary mobility is controlled by decomposing the kink, atom diffusion along the step and grain boundary surface, and the condensation process on another grain boundary. The possible reason of the triple junction dragging effect is the sluggish nucleation of a new step and a kink site on the growing grain boundary, i.e., the sluggish condensation process on the new grain boundary as reported by Chen et al. [37].

Another possible factor potentially impacting the kinetics of grain growth is impurity on the samples' grain boundary. Trace amount of oxygen may be trapped on the powder surfaces and at the grain boundaries during sintering and isothermal annealing. However, it is challenging to determine the oxygen level in the metallic powders and sintered pellets for grain growth study as a result of the pyrophoric nature of metallic powders and surface oxidation of sintered pellets once removed from the oxygen controlled environment, as shown in the XRD patterns (Fig. 2). The oxide phase may have potential influence on the grain growth kinetics, playing a role in retarding the grain growth as the secondary phase existing on the grain boundary [38]. To mitigate this impact, in this study, the handling of metallic U powders was conducted inside the environmentally-controlled glovebox with low oxygen level (< 10 ppm). The sintering and consolidation of metallic pellets and isothermal-annealing were carefully handled to avoid possible oxidation. A highly oxygen-depleted environment was applied during isothermal annealing with a piece of Ta foil loaded inside the quartz tube heated to around 1273 K to absorb the residual oxygen inside the tube. The oxygen partial pressure during isothermal annealing is estimated around 1.42×10^{-22} bar [39]. Therefore, the activation energy for grain growth determined for pure gamma phase uranium in this study may represent the best estimate of the value that could be achieved, and an accurate determination of the oxygen level with the minimized sources of uncertainties could be useful to clarify the role of the possible oxygen impurity on the grain growth kinetics.

5. Conclusions

In summary, the grain growth mechanisms and kinetics of pure gamma phase uranium with different grain structures were systematically investigated by isothermal annealing at different temperatures and durations. The uranium samples with different grain sizes (varying from nano-sized and submicron-sized) were fabricated by combining high-energy ball milling and SPS consolidation. Post thermal treatments was conducted on the SPS consolidated samples to control the grain structure and crystallinity. Our results indicate that the grain structure has a significant impact on the grain growth kinetics and mechanisms. The submicron-sized gamma uranium displays a parabolic relation between sample size and annealing duration, dominated by the grain boundary movement. In contrast, the nano-sized gamma uranium phase shows a linear relation, and the grain growth mechanism is dominated by the triple junction movement. The grain growth activation energies are determined as 80.6 KJ/mol and 199.5 KJ/mol for the submicron-sized and nano-sized gamma uranium, respectively. With the grain growth, the grain shape changed from quadrilateral grain geometry to the round geometry and then the grain growth mechanism transits from triple junction movement to grain boundary diffusion. These grain growth kinetics and activation energies allow an understanding of the pore and grain structure evolution of metallic fuels induced by thermally-dominated processes, which are necessary for the prediction of the metallic fuel behavior induced by radiation under relevant reactor operation conditions.

U.S. Department of energy disclaimer

information, apparatus, product, or process disclosed, or represents that its use would not infringe privately owned rights. References herein to any specific commercial product, process, or service by trade name, trademark, manufacturer, or otherwise, does not necessarily constitute or imply its endorsement, recommendation, or favoring by the U.S. Government or any agency thereof. The views and opinions of authors expressed herein do not necessarily state or reflect those of the U.S. Government or any agency thereof.

Declaration of Competing Interest

The authors declare that they have no known competing financial interests or personal relationships that could have appeared to influence the work reported in this paper.

CRediT authorship contribution statement

Dong Zhao: Formal analysis, Investigation, Writing – original draft, Visualization. **Michael T. Benson:** Resources, Writing – review & editing. **Kun Yang:** Investigation, Writing – review & editing. **Yonglin Huang:** Investigation, Writing – review & editing. **Fidelma G. Di Lemma:** Resources, Writing – review & editing. **Bowen Gong:** Formal analysis, Writing – review & editing. **Fudong Han:** Investigation, Writing – review & editing. **Jie Lian:** Conceptualization, Funding acquisition, Resources, Writing – review & editing.

Data availability

Data will be made available on request.

Acknowledgement

This work was supported by the U.S. Department of Energy, Office of Nuclear Energy under DOE Idaho Operations Office Contract DE-AC07–05ID14517, through Laboratory Directed Research and Development (LDRD) and DOE ARPA-E under award # 18/CJ000/15/05. Accordingly, the U.S. Government retains and the publisher, by accepting the article for publication, acknowledges that the U.S. Government retains a nonexclusive, paid-up, irrevocable, worldwide license to publish or reproduce the published form of this manuscript or allow others to do so, for U.S. Government purposes.

References

[1] D.C. Crawford, D.L. Porter, S.L. Hayes, Fuels for sodium-cooled fast reactors: US perspective, J. Nucl. Mater. 371 (2007) 202–231, doi:10.1016/j.jnucmat.2007.05.010.
[2] C. Matthews, C. Unal, J. Galloway, D.D. Keiser, S.L. Hayes, Fuel-cladding chemical interaction in U-Pu-Zr metallic fuels: a critical review, Nucl. Technol. 198 (2017) 231–259, doi:10.1080/00295450.2017.1323535.
[3] T. Ogata, Metal Fuel, in: Compr. Nucl. Mater., Elsevier, 2012, pp. 1–40, doi:10.1016/B978-0-08-056033-5.00049-5.
[4] W.J. Carmack, D.L. Porter, Y.I. Chang, S.L. Hayes, M.K. Meyer, D.E. Burkes, C.B. Lee, T. Mizuno, F. Delage, J. Somers, Metallic fuels for advanced reactors, J. Nucl. Mater. 392 (2009) 139–150, doi:10.1016/j.jnucmat.2009.03.007.
[5] X. Liu, L. Capriotti, T. Yao, J.M. Harp, M.T. Benson, Y. Wang, F. Teng, L. He, Fuel-cladding chemical interaction of a prototype annular U-10Zr fuel with Fe-12Cr ferritic/martensitic HT-9 cladding, J. Nucl. Mater. 544 (2021) 152588, doi:10.1016/j.jnucmat.2020.152588.
[6] T. Yao, L. Capriotti, J.M. Harp, X. Liu, Y. Wang, F. Teng, D.J. Murray, A.J. Winston, J. Gan, M.T. Benson, L. He, α-U and ω-UZr2 in neutron irradiated U-10Zr annular metallic fuel, J. Nucl. Mater. 542 (2020) 152536, doi:10.1016/j.jnucmat.2020.152536.
[7] Y.S. Kim, G.L. Hofman, S.L. Hayes, Y.H. Sohn, Constituent redistribution in U–Pu–Zr fuel during irradiation, J. Nucl. Mater. 327 (2004) 27–36, doi:10.1016/j.jnucmat.2004.01.012.
[8] G. Beghi, Gamma phase uranium-molybdenum fuel alloys, (n.d.) 90.
[9] H.L. Yakel, A review of X-ray diffraction studies in uranium alloys, (n.d.) 53.
[10] Y. Adda, A. Kirianenko, Etude de l'autodiffusion de l'uranium en phase γ, J. Nucl. Mater. 1 (1959) 120–126, doi:10.1016/0022-3115(59)90045-5.
[11] P.E. Armstrong, D.T. Eash, J.E. Hockett, Elastic moduli of alpha, beta and gamma polycrystalline uranium, J. Nucl. Mater. 45 (1972) 211–216, doi:10.1016/0022-3115(72)90167-5.
[12] S.L. Robinson, O.D. Sherby, P.E. Armstrong, Elevated temperature plastic flow of high purity uranium in the alpha, beta and gamma phases, J. Nucl. Mater. 46 (1973) 293–302, doi:10.1016/0022-3115(73)90044-5.
[13] M. Aizenshtein, E. Brosh, Z. Ungarish, S. Levi, M. Tubul, D. Fadel, E. Greenberg, S. Hayun, High entropy uranium-based alloys: thermodynamics, characterization and mechanical properties, J. Nucl. Mater. 558 (2022) 153378, doi:10.1016/j.jnucmat.2021.153378.
[14] T. Yao, K. Mo, D. Yun, S. Nanda, A.M. Yacout, J. Lian, Grain growth and pore coarsening in dense nano-crystalline UO $_{2+x}$ fuel pellets, J. Am. Ceram. Soc. 100 (2017) 2651–2658, doi:10.1111/jace.14780.
[15] B. Gong, T. Yao, P. Lei, J. Harp, A.T. Nelson, J. Lian, Spark plasma sintering (SPS) densified U3Si2 pellets: microstructure control and enhanced mechanical and oxidation properties, J. Alloys Compd. 825 (2020) 154022, doi:10.1016/j.jallcom.2020.154022.
[16] K. Yang, E. Kardoulaki, D. Zhao, A. Broussard, K. Metzger, J.T. White, M.R. Sivack, K.J. Mcclellan, E.J. Lahoda, J. Lian, Uranium nitride (UN) pellets with controllable microstructure and phase – fabrication by spark plasma sintering and their thermal-mechanical and oxidation properties, J. Nucl. Mater. 557 (2021) 153272, doi:10.1016/j.jnucmat.2021.153272.
[17] D.A. Young, Phase Diagrams of the Elements, Lawrence Livermore National Lab. (LLNL), Livermore, CA (United States), 1975, doi:10.2172/4010212.
[18] G. Kimmel, X-Ray Diffraction (XRD) Characteri- zation of microstrain in some iron and uranium alloys, Annu. Rep. 29 (1996).
[19] J. Wormhoudt, Uranium Oxide Gaseous Ion and Neutral Infrared Spectroscopy, Defense Technical Information Center, Fort Belvoir, VA, 1983, doi:10.21236/ADA156032.
[20] K.C. Hartig, S.S. Harilal, M.C. Phillips, B.E. Brumfield, I. Jovanovic, Evolution of uranium monoxide in femtosecond laser-induced uranium plasmas, Opt. Express. 25 (2017) 11477–11490, doi:10.1364/OE.25.011477.
[21] Y. Estrin, G. Gottstein, E. Rabkin, L.S. Shvindlerman, Grain growth in thin metallic films, Acta Mater 49 (2001) 673–681, doi:10.1016/S1359-6454(00)00344-X.
[22] C.E. Krill, L. Helfen, D. Michels, H. Natter, A. Fitch, O. Masson, R. Birringer, Size-dependent grain-growth kinetics observed in nanocrystalline Fe, Phys. Rev. Lett. 86 (2001) 842–845, doi:10.1103/PhysRevLett.86.842.
[23] T.R. Malow, C.C. Koch, Grain growth in nanocrystalline iron prepared by mechanical attrition, Acta Mater 45 (1997) 2177–2186, doi:10.1016/S1359-6454(96)00300-X.
[24] F.J. Gil, J.A. Planell, Behaviour of normal grain growth kinetics in single phase titanium and titanium alloys, Mater. Sci. Eng. A. 283 (2000) 17–24, doi:10.1016/S0921-5093(00)00731-0.
[25] M.A. Fortes, Grain growth kinetics: the grain growth exponent, Mater. Sci. Forum. 94–96 (1992) 319–324, doi:10.4028/www.scientific.net/MSF.94-96.319.
[26] N.L. Peterson, S.J. Rothman, Diffusion in gamma uranium, Phys. Rev. 136 (1964) A842–A848, doi:10.1103/PhysRev.136.A842.
[27] H.S. Levine, C.J. MacCallum, Grain boundary and lattice diffusion in polycrystalline bodies, J. Appl. Phys. 31 (2004) 595, doi:10.1063/1.1735634.
[28] R.E. Hoffman, D. Turnbull, Lattice and grain boundary self-diffusion in silver, J. Appl. Phys. 22 (1951) 634–639, doi:10.1063/1.1700021.
[29] Y. Estrin, G. Gottstein, E. Rabkin, L.S. Shvindlerman, On the kinetics of grain growth inhibited by vacancy generation, Scr. Mater. 43 (2000) 141–147, doi:10.1016/S1359-6462(00)00383-3.
[30] G. Gottstein, A.H. King, L.S. Shvindlerman, The effect of triple-junction drag on grain growth, Acta Mater 48 (2000) 397–403, doi:10.1016/S1359-6454(99)00373-0.
[31] C. Saldana, T.G. Murthy, M.R. Shankar, E.A. Stach, S. Chandrasekar, Stabilizing nanostructured materials by coherent nanotwins and their grain boundary triple junction drag, Appl. Phys. Lett. 94 (2009) 021910, doi:10.1063/1.3072595.
[32] V.G. Sursaeva, L.S. Shvindlerman, G. Gottshtain, Features of migration of triple junctions of different configuration, Bull. Russ. Acad. Sci. Phys. 71 (2007) 1697–1701, doi:10.3103/S106287380712009X.
[33] G. Gottstein, Y. Ma, L. Shvindlerman, Triple junction motion and grain microstructure evolution, Acta Mater 53 (2005) 1535–1544, doi:10.1016/j.actamat.2004.12.006.
[34] U. Czubayko, V.G. Sursaeva, G. Gottstein, L.S. Shvindlerman, Influence of triple junctions on grain boundary motion, Acta Mater 46 (1998) 5863–5871, doi:10.1016/S1359-6454(98)00241-9.
[35] G. Gottstein, L.S. Shvindlerman, Triple junction drag and grain growth in 2D polycrystals, Acta Mater 50 (2002) 703–713, doi:10.1016/S1359-6454(01)00391-3.
[36] H. Gleiter, Theory of grain boundary migration rate, Acta Metall 17 (1969) 853–862, doi:10.1016/0001-6160(69)90105-9.
[37] K.-C. Chen, W.-W. Wu, C.-N. Liao, L.-J. Chen, K.N. Tu, Observation of Atomic Diffusion at Twin-Modified Grain Boundaries in Copper, Science 321 (2008) 1066–1069, doi:10.1126/science.1160777.
[38] K. Chang, W. Feng, L.-Q. Chen, Effect of second-phase particle morphology on grain growth kinetics, Acta Mater 57 (2009) 5229–5236, doi:10.1016/j.actamat.2009.07.025.
[39] H.S. Hong, Y.S. Kim, A thermodynamic study of the tantalum-oxygen system., 2001. https://doi.org/10.2172/786921.